Spatially separated skin effect and edge states in one-dimensional semi–Su-Schrieffer-Heeger lattices

Jia-Rui Li,[1] Lian-Lian Zhang,[1] Chen-Hao Zhao,[1] Shu-Feng Zhang,[2] Yu-Lian Zhu,[1] and Wei-Jiang Gong[1,*]

[1]*College of Sciences, Northeastern University, Shenyang 110819, China*

[2]*School of Physics and Technology, University of Jinan, Jinan 250022, China*

(Received 8 December 2023; revised 28 February 2024; accepted 21 March 2024; published 3 April 2024)

We investigate the skin effect and topological properties in the one-dimensional semi–Su-Schrieffer-Heeger (semi–SSH) lattice, in which the intersite couplings in one direction are uniform but in the other direction the intersite couplings change alternately. Following the detailed theoretical demonstration, we find that in this system, the skin effect can be tunable by adjusting the magnitudes of the intersite couplings in the two directions. However, the change of the skin effect does not necessarily modulate the topological edge states, and such two phenomena are allowed to appear in a spatially separated way. Therefore, we propose one scheme to change the directionality of the topological edge states and the localized bulk states, by controlling the intersite couplings. This promotes the understanding of the skin effects and topological properties in the one-dimensional SSH lattices with nonreciprocal couplings.

DOI: 10.1103/PhysRevB.109.165407

I. INTRODUCTION

Non-Hermitian systems, characterized by their non-Hermitian Hamiltonians, have attracted much attention both theoretically and experimentally [1–5]. At present, lots of groups have devoted themselves to the non-Hermitian systems, by introducing gain and loss potentials [6–9] or considering the nonreciprocal couplings [10–12]. Moreover, the non-Hermitian systems have the wealth of applications in optics and photonics systems [13–16], topological lasers [17], and enhanced sensing [18–20].

Regarding the non-Hermitian systems with nonreciprocal coupling terms, one of the important features lies in the fact that the system has non-Hermitian skin effect [21–24]. The appearance of the non-Hermitian skin effect marks the complete breakdown of the bulk-boundary correspondence [21,22,25]. This indicates that topological invariants under periodic boundary condition cannot describe the topological properties of nonreciprocal coupled systems. Such a phenomenon has attracted the interest from the theoretical physicists, and the non-Bloch energy band theory has been proposed to describe the underlying topology [21], with the help of the concepts of generalized Brillouin zone (GBZ) [26–28], non-Bloch bulk-boundary correspondence [21], and non-Bloch topological invariants [21,26]. Meanwhile, non-Hermitian skin effects have been realized experimentally, including cold atoms, quantum optical systems, optical grid systems [29–32], topolectrical circuit [33], and photonic systems [34].

In view of the research about the nonreciprocal systems, the Su-Schrieffer-Heeger (SSH) lattice is one typical and important candidate for discussing interplay between the topological phenomena and non-Hermitian skin effect [28,35,36]. However, so far few literatures have demonstrated the relation between the skin effect of bulk states and the localization of the edge states. In this work, we aim to investigate the spatially separated skin effect and edge states in the 1D semi–SSH lattice, in which the intersite coupling in one direction is uniform but in the other direction the intersite couplings change alternately. Following the detailed theoretical demonstration, we find that in this system, the skin effect can be tunable by adjusting the magnitudes of the intersite couplings in the two directions. However, the change of the skin effect does not necessarily modulate the topological edge states. Therefore, in this work we propose one scheme to change the directionality of the topological edge states and the localized bulk states, by controlling the intersite couplings. This promotes the understanding of the skin effects and topological properties in the 1D SSH lattices with nonreciprocal couplings.

II. MODEL AND THEORY

We propose a one-dimensional spinless particle structure with direction-dependent intersite coupling terms, which consists of N units, as shown in Fig. 1(a). The Hamiltonian of the semi–SSH model can be written as

$$H = \sum_m (t a_m^\dagger b_m + t_1 b_m^\dagger a_m + t b_m^\dagger a_{m+1} + t_2 a_{m+1}^\dagger b_m), \quad (1)$$

where $\alpha_m^\dagger$ and $\alpha_m [\alpha \in (a, b)]$ are the creation and annihilation operators in the mth cell. t denotes the hopping term from right to left, and t_1 and t_2 are the other type of hopping terms, respectively. In this work, we assume $t_1 = t_0 + \delta \cos\theta$ and $t_2 = t_0 - \delta \cos\theta$, which represent the intracell and intercell hopping terms from left to right. Here $\theta \in (0, 2\pi)$ is the phase parameter and $\delta \in (0, 1)$ describes the strength of dimerization.

*gwj@mail.neu.edu.cn

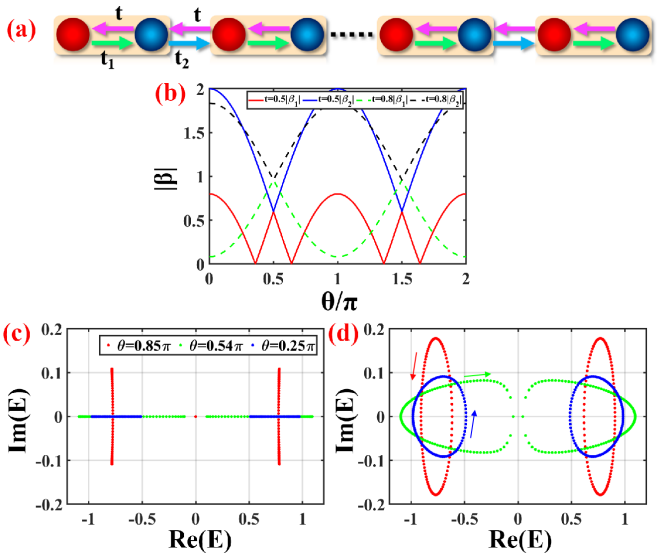

FIG. 1. (a) Illustration of the semi-SSH structure. (b) Specific results of $|\beta_1|$ and $|\beta_2|$ as the change of θ where the red-blue (green-black) line denotes the case of $t = 0.5$ ($t = 0.8$). (c) Energy spectra $\mathrm{Re}(E) - \mathrm{Im}(E)$ in the OBC. The blue, green, and red points describe the cases of $\theta = 0.25\pi$, $\theta = 0.45\pi$, and $\theta = 0.85\pi$, respectively. (d) The energy spectra $\mathrm{Re}(E) - \mathrm{Im}(E)$ in the PBC. The blue, green, and red points denote the cases of $\theta = 0.25\pi$, $\theta = 0.45\pi$, and $\theta = 0.85\pi$, respectively. The arrows indicate the direction of rotation, where red and blue colors are counterclockwise and green is clockwise. Other parameters are set as $t = 0.5$, $t_0 = 0.6$, and $\delta = 0.7$.

By using the Fourier transformation, the Hamiltonian in the momentum space can be obtained, i.e.,

$$H(k) = \begin{bmatrix} 0 & t + t_2 e^{-ik} \\ t_1 + t e^{ik} & 0 \end{bmatrix}. \tag{2}$$

We can also write the Hamiltonian by Pauli matrices, i.e., $H(k) = (t + t_2 e^{-ik})\sigma_+ + (t_1 + t e^{ik})\sigma_-$, where $\sigma_+ = (\sigma_x + i\sigma_y)/2$ and $\sigma_- = (\sigma_x - i\sigma_y)/2$ with $\sigma_{x,y}$ being the Pauli matrices.

A. Symmetry

Regarding this Hamiltonian, we would like to first discuss the symmetry to infer the topological properties. For our model, it can be first found that the system has the time-reversal symmetry (TRS†), i.e., $\mathcal{T}H^T\mathcal{T}^{-1} = H$, with $\mathcal{T} = \mathrm{offdiag}(1, 1, \ldots)_{2N}$. Also, the system has the particle-hole symmetry (PHS†) $\mathcal{C}H^*\mathcal{C}^{-1} = -H$, with the corresponding operator being $\mathcal{C} = \mathrm{offdiag}(1, -1, 1, \ldots)_{2N}$. The existence of PHS† implies that the energy eigenvalues are symmetric about $E = 0$ [37]. In addition to the two symmetries above, one can see that the chiral symmetry (CS) exists in this system, where $\Gamma H \Gamma^{-1} = -H$ and $\Gamma = \mathrm{offdiag}(1, -1, 1, \ldots)_{2N}$. According to the classification of symmetry [38], the system belongs to the BDI† and has the Z-class topological invariant. Moreover, the system also has the pseudo-Hermitian symmetry $\eta H \eta^{-1} = H^\dagger$, where $\eta = \mathrm{diag}(1, \frac{t}{t_1}, \frac{t^2}{t_1 t_2}, \cdots, \frac{t^{(2N-1)}}{t_1^{(2N-2)} t_2^{(2N-3)}})$. The existence of pseudo-Hermitian symmetry signifies that the system could have the real energy states [39,40]. All the real energies are located in the protected pseudo-Hermitian symmetric phase (PPHS). In the presence of the imaginary part of energy, pseudo-Hermitian symmetry will be broken, and then we can consider the system to be in the broken pseudo-Hermitian symmetric phase (BPHS).

B. Topological phase condition

Based on the conclusions in the previous works [11,21,22,41,42], the nonreciprocal coupling can destroy the bulk-boundary condition. This result leads to the fact that the topological phase transitions calculated with periodic boundary conditions (PBC) do not correspond to the energy spectra with open boundary conditions (OBC). Therefore, we have to calculate the topological phase transition in OBC by a generalizable solution in the generalized Brillouin zone [21,22]. According to the Schrödinger equation $H|\Psi\rangle = E|\Psi\rangle$ in which $|\Psi\rangle = (\psi_{a,1}, \psi_{b,1}, \psi_{a,2} \ldots, \psi_{a,N}, \psi_{b,N})^T$, we can get the relationship of the bulk-state equations:

$$\begin{aligned} t_2\psi_{b,m+1} + t\psi_{b,m} &= E\psi_{a,m}, \\ t_1\psi_{a,m} + t\psi_{a,m+1} &= E\psi_{b,m}, \end{aligned} \tag{3}$$

where $\psi_{a,m} = \sum_s \beta_s^m \phi_a^{(s)}$ and $\psi_{b,m} = \sum_s \beta_s^m \phi_b^{(s)}$. N is the number of unit cells. Substituting it into Eq. (3), we can obtain the bulk-state eigenequation:

$$\begin{aligned} (t + t_2\beta_s^{-1})\phi_b^{(s)} &= E\phi_a^{(s)}, \\ (t_1 + t\beta_s)\phi_a^{(s)} &= E\phi_b^{(s)}. \end{aligned} \tag{4}$$

Then, we can get the expression between E and β_s:

$$(t + t_2\beta_s^{-1})(t_1 + t\beta_s) = E^2. \tag{5}$$

Besides, according to Eq. (4), we can determine the relationship satisfied between $\phi_a^{(s)}$ and $\phi_b^{(s)}$: $\phi_b^{(s)} = \frac{E}{t+t_2\beta_s^{-1}}\phi_a^{(s)}$ and $\phi_a^{(s)} = \frac{E}{t_1+t\beta_s}\phi_b^{(s)}$. Since Eq. (4) is the quadratic equation, the equation could have two solutions. Thus, the index s can be set as $s = (1, 2)$.

The two solutions β_s of Eq. (5) can be expressed as

$$\beta_{1(2)}(E) = \frac{-\Delta \pm \sqrt{\Delta^2 - 4t^2 t_1 t_2}}{2t^2} \tag{6}$$

with $\Delta = tt_1 + tt_2 - E^2$. Under the condition of $E \to 0$, the two solutions can be simplified, i.e.,

$$\beta_{1(2)}(0) = -\frac{t_1 + t_2 \pm |t_1 - t_2|}{2t}. \tag{7}$$

This means that $\beta_1\beta_2 = \frac{t_1 t_2}{t^2}$. Moreover, if $t_1 > t_2$, there will be $\beta_1 = -t_1/t$ and $\beta_2 = -t_2/t$; if $t_1 < t_2$, one can find the result that $\beta_1 = -t_2/t$ and $\beta_2 = -t_1/t$.

Next we focus on the boundary condition. According to the Hamiltonian, we can get the expressions of the boundary condition as

$$t\psi_{b,1} = E\psi_{a,1} \quad \text{and} \quad t_1\psi_{a,N} = E\psi_{b,N}. \tag{8}$$

Similar to the bulk states, we can also get the expressions $(\psi_{a,m}, \psi_{b,m}) = (\phi_{a,m}^{(1)}, \phi_{b,m}^{(1)}) + (\phi_{a,m}^{(2)}, \phi_{b,m}^{(2)}) = \beta_1^m(\phi_a^{(1)}, \phi_b^{(1)}) + \beta_2^m(\phi_a^{(2)}, \phi_b^{(2)})$. Substituting the expression into Eq. (8), the equation can be expressed as $t(\beta_1\phi_b^{(1)} +$

$\beta_2\phi_b^{(2)}) - E(\beta_1\phi_a^{(1)} + \beta_2\phi_a^{(2)}) = 0$ and $t_1(\beta_1^L\phi_a^{(1)} + \beta_2^L\phi_a^{(2)}) - E(\beta_1^L\phi_b^{(1)} + \beta_2^L\phi_b^{(2)}) = 0$. According to the relation $\phi_a^{(s)} = \frac{E}{t_1+t\beta_s}\phi_b^{(s)}$ $(s = 1, 2)$, we obtain the result that $t(\beta_1\phi_b^{(1)} + \beta_2\phi_b^{(2)}) - E[\beta_1\frac{E}{t_1+t\beta_1}\phi_b^{(1)} + \beta_2\frac{E}{t_1+t\beta_2}\phi_b^{(2)}] = 0$ and $t_1[\beta_1^L\frac{E}{t_1+t\beta_1}\phi_b^{(1)} + \beta_2^L\frac{E}{t_1+t\beta_2}\phi_b^{(2)}] - E(\beta_1^L\phi_b^{(1)} + \beta_2^L\phi_b^{(2)}) = 0$. Based on the above expression, the following relationship can be written out:

$$\phi_b^{(1)} = -\phi_b^{(2)},$$
$$-\frac{t\beta_1^{N+1}}{t_1+t\beta_1}\phi_b^{(1)} - \frac{t\beta_2^{N+1}}{t_1+t\beta_2}\phi_b^{(2)} = 0. \tag{9}$$

Thus, the equation $\beta_1^{N+1}(t_1 + t\beta_2) = \beta_2^{N+1}(t_1 + t\beta_1)$ can be obtained. In the limit of $N \to \infty$ and $E \to 0$, we can solve the topological phase transition conditions in the GBZ in the case of $|\beta_1| = |\beta_2|$. Accordingly, the exact topological phase transition condition can be written as

$$\left|\beta_1^{E\to 0}\right| = \left|\beta_2^{E\to 0}\right| = r \Rightarrow t_1 = t_2. \tag{10}$$

According to the assumption $t_{1(2)} = t_0 \pm \delta\cos\theta$, such a condition can be simplified as $\theta = (2s-1)\pi/2$ $(s = 0, 1, \ldots)$ under the condition of $\delta \neq 0$. Besides, we can find that the phase transition condition is independent of the hopping parameter t. In Fig. 1(b), we plot the spectra of $|\beta| - \theta$, and see that the curves of $|\beta_1|$ and $|\beta_2|$ are closed at $\theta = 0.5\pi$ (1.5π) when $t = 0.5$. What should be notable is that the critical point is unchanged when t is increased to 0.8.

C. Conditions of pseudo-Hermitian symmetric phase transition and skin effect transition

In order to observe the difference in the energy band structures between the two boundary conditions, Figs. 1(c) and 1(d) show the energy spectra $\mathrm{Re}(E) - \mathrm{Im}(E)$ of the system under OBC and PBC, respectively. In this figure, the blue, green, and red colors respectively show the cases of $\theta = 0.25\pi$, $\theta = 0.45\pi$, and $\theta = 0.85\pi$. Comparing the energy spectra under the two boundaries, it can be clearly found that the energy spectra under the two boundary conditions cannot correspond no matter how θ changes. This result marks the breaking of the bulk-boundary correspondence, which is consistent with the previous discussion. Accordingly, the system is able to display the non-Hermitian skin effect.

From the spectra of OBC in Fig. 1(c), we can clearly find that the eigenenergies are real in the case of $\theta = 0.25\pi$ (0.45π), which is consistent with the symmetry property. When θ is changed to $\theta = 0.85\pi$, the eigenvalues have the imaginary part, i.e., $\mathrm{Im}(E) \neq 0$, and the system enters the BPHS phase. These results indicate that the system undergoes the pseudo-Hermitian symmetric phase transition.

Next, we focus on the complex spectrum plane in the PBC. According to the previous work [43], we can infer the local direction by observing the direction of rotation of the energy spectrum. In Fig. 1(d), we display the energy spectra and rotation direction as θ changes. Specifically, in the case of $\theta = 0.25\pi$, there are two loops that appear in the complex energy plane [blue]. Take the left loop with the negative real part of energy as an example, we see that when the eigenenergies of respective states undergo the process of $(\mathrm{Re}(E), \mathrm{Im}(E)) = (-0.982, 0) \to (-0.486, 0) \to (-0.982, 0)$, the signs of the imaginary part of energy constructs the $0 \to [\mathrm{Im}(E) < 0] \to 0 \to [\mathrm{Im}(E) > 0] \to 0$ loop according to the sequence of such states. This indicates that the system shows the counterclockwise process, and all the bulk states could be localized on the left side. For the case of $\theta = 0.45\pi$ [green], the imaginary part of energy produces the $0 \to [\mathrm{Im}(E) > 0] \to 0 \to [\mathrm{Im}(E) < 0] \to 0$ sequence with the change of $(\mathrm{Re}(E), \mathrm{Im}(E)) = (-0.906, 0) \to (-0.616, 0) \to (-0.906, 0)$. Thus, the direction of rotation shifts to clockwise and the local direction turns to the right side. When θ becomes equal to $\theta = 0.85\pi$ [red], the sequence direction changes to the same as the case of $\theta = 0.25\pi$ during the change of $(\mathrm{Re}(E), \mathrm{Im}(E)) = (-1.095, 0) \to (-0.045, 0) \to (-1.095, 0)$. The localization occurs on the left side again. The change in the energy spectrum from the counterclockwise to clockwise rotational means the transition in the skin effect, i.e., the localization direction of the bulk states shift from the left to the right site.

To better judge the two types of phase transition processes, we would like to calculate their critical conditions. On the one hand, we focus on the condition of the pseudo-Hermitian symmetric phase transition.For the pseudo-Hermitian symmetric phase transition, he products of upper and lower subdiagonal are positive then all eigenvalues of H are real [40]. In our model, the critical conditions are $tt_1 > 0$ and $tt_2 > 0$, respectively. Therefore, the condition of pseudo-Hermitian symmetric phase transition is manifested as

$$\begin{cases} \cos^2\theta < t_0^2/\delta^2, & \text{PPHS phase,} \\ \cos^2\theta > t_0^2/\delta^2, & \text{BPHS phase.} \end{cases} \tag{11}$$

We can get the results that the system is a PPHS phase when $\theta \in [0, \arccos(\frac{t_0}{\delta})] \cup [\arccos(-\frac{t_0}{\delta}), \pi + \arccos\frac{t_0}{\delta}] \cup [\pi + \arccos(-\frac{t_0}{\delta}), 2\pi]$, and it is a BPHS phase for $\theta \in [\arccos\frac{t_0}{\delta}, \arccos(-\frac{t_0}{\delta})] \cup [\pi + \arccos\frac{t_0}{\delta}, \pi + \arccos(-\frac{t_0}{\delta})]$. Similarlu, we can get the same results from Eq. (3) [21]. Substituting $\beta = re^{ik}$ into Eq. (3), we can get the relationship that $E^2(k) = tt_1 + tt_2 + \sqrt{|t^2t_1t_2|}\mathrm{sgn}(t^2)e^{ik} + \sqrt{|t^2t_1t_2|}\mathrm{sgn}(t_1t_2)e^{-ik}$. Surely, the system energies are real when $t_1t_2 > 0$.

On the other hand, we would like to calculate the condition of skin effect transition. According to the works of Wang [22], the eigenstates are localized at the right (left) boundary when $r > 1 (r < 1)$. For our model, $r = \sqrt{|t_1t_2/t^2|}$, so the condition of skin effect can be transited, i.e.,

$$\begin{cases} t^2 < \left|t_0^2 - \delta^2\cos^2\theta\right|, & \text{right direction,} \\ t^2 > \left|t_0^2 - \delta^2\cos^2\theta\right|, & \text{left direction.} \end{cases} \tag{12}$$

III. NUMERICAL RESULTS AND DISCUSSIONS

Based on the above theoretical analysis, we know that the system has an opportunity to undergo the skin-effect transition with the change of hopping parameters. Thus, we would like to introduce directional inverse participation ratio χ with its

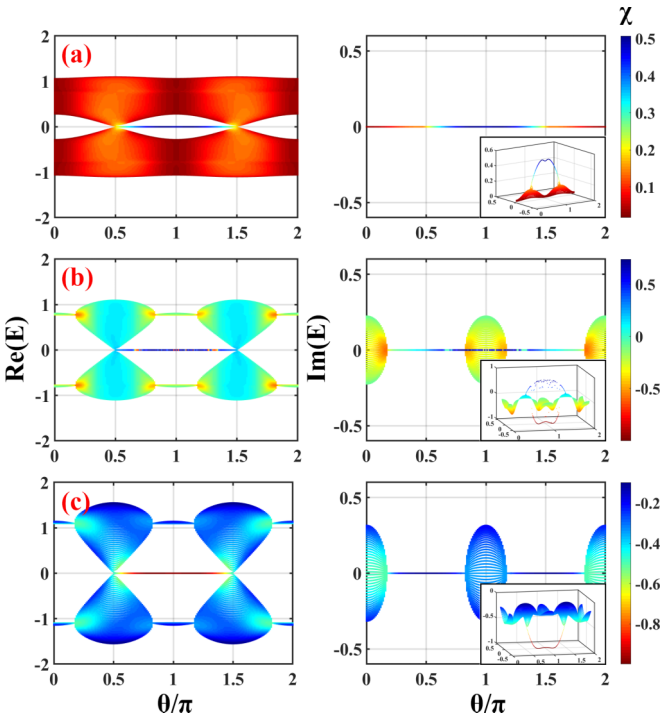

FIG. 2. (a)–(c) The real and imaginary energy spectra of $(t, \delta) = (0.5, 0.3)$, $(t, \delta) = (0.5, 0.7)$, and $(t, \delta) = (1, 0.7)$. The color indicates the value of χ. The left column is the real part of the eigenenergies, and the right column is the corresponding imaginary part. The inset in the right column shows the three-dimensional view of the energy spectrum of the imaginary part.

definition equation being [44]

$$\chi_n = \mathrm{sgn}\left[\sum_{j=1}^{L}\left(j - \frac{L}{2} - \gamma\right)|\psi_{n,j}|\right]\frac{\sum_j |\psi_{n,j}|^4}{\left(\sum_j |\psi_{n,j}|^2\right)^2}. \quad (13)$$

In this expression, $|\psi_{n,j}\rangle$ is the jth eigenstate of eigenvalue E_n. $L = 2N$ is the number of total sublattices. γ is a constant and usually set as $0 < \gamma < 0.5$. $\mathrm{sgn}(x)$ is the sign function. $\frac{\sum_j |\psi_{n,j}|^4}{(\sum_j |\psi_{n,j}|^2)^2}$ is the definition of the inverse participation rate and it can display the localization of states. By observing the value of χ_n to be positive or negative, one can determine whether the wavefunction of the nth eigenstate has a tendency to be right local or left local. In addition, when the value of χ_n is close to zero, the system will be localized in both the left and right directions.

In order to observe the energy nature of the system under the OBC, we plot the real and imaginary energy spectra of $(t, \delta) = (0.5, 0.3)$, $(t, \delta) = (0.5, 0.7)$, and $(t, \delta) = (1, 0.7)$ with $t_0 = 0.6$ in Fig. 2. The color represents the value of χ. The left column is the real part of the eigenenergies, and the right column is the corresponding imaginary part. The insets in the three cases of the right column show the three-dimensional view of the energy spectrum of the imaginary part, which can help us to better observe the values χ of the topological zero-energy edge states (for simplicity, topological states) and the critical value of transition.

In the case of $(t, \delta) = (0.5, 0.3)$, the result in Fig. 2(a) shows that all eigenenergies are real because the system satisfies $\cos^2\theta < t_0^2/\delta^2 = 4$ as θ changes. The topological states exist in the region of $\theta \in (0.5\pi, 1.5\pi)$. The value of χ also suggests that regardless of bulk states or topological states, χ is always larger than zero. This means that all eigenstates display the trend of right-side localization. Figure 2(b) describes the case of $(t, \delta) = (0.5, 0.7)$. One can find that the system has different phenomena in such a case. To be specific, for the bulk states, the system undergoes the pseudo-Hermitian symmetric phase transition at $\theta = 0.17\pi\,(1.17\pi)$ and $0.83\pi\,(1.83\pi)$. The imaginary energy appears in the region of $\theta \in [0, 0.17\pi] \cup [0.83\pi, 1.17\pi] \cup [1.83\pi, 2\pi]$, these states are BPHS phases. $\theta \in [0.17\pi, 0.83\pi] \cup [1.17\pi, 1.83\pi]$ is the PPHS phase where $\mathrm{Im}(E) = 0$. Besides, $\chi > 0$ of the bulk states arises in the region of $\theta \in [0.34\pi, 0.65\pi] \cup [1.34\pi, 1.65\pi]$. This indicates that the bulk states could be localized at the right boundary. In the region of $\theta \in [0, 0.34\pi] \cup [0.65, 1.34\pi] \cup [1.65\pi, 2\pi]$, the bulk states could be localized on the left side because of $\chi < 0$. These results are consistent with Eq. (10) and Eq. (11). For the topological states, the range of them are also manifested as $0.5\pi < \theta < 1.5\pi$ and the eigenenergies are purely real. In contrast with case of the Fig. 2(a), when $0.5\pi < \theta < 0.67\pi\,(1.33\pi < \theta < 1.5\pi)$, the values of χ of the two topological states are both greater than zero, so the two topological states are localized on the right side. However, in the region of $0.67\pi < \theta < 1.33\pi$, one topological state is $\chi > 0$ and the other is $\chi < 0$ in the region of $0.67\pi < \theta < 1.33\pi$. This phenomenon means that the topological states have the double side localization effects, i.e., one could be localized on the left side and the other is localized right. Besides, the value of $|\chi|$ of topological states are lager than bulk states, which means that the localization of topological states is stronger than bulk states. When changing the magnitude of t, such as the case of $(t, \delta) = (1.0, 0.7)$ in Fig. 2(c), we see that the conditions of pseudo-Hermitian symmetric phase transition are $\theta = 0.17\pi\,(1.17\pi)$ and $\theta = 0.83\pi\,(1.83\pi)$, respectively. The topological states are still purely real. From the values of χ, we can find that they are less than zero. $|\chi|$ of topological states are identical for the same θ, which is larger than those of the bulk states. One can then understand that all eigenstates have the trend to be localized at the left boundary, and the localization of topological states is stronger than bulk states.

Up to now, we can conclude that the system has three different phase transitions: topological phase transition, pseudo-Hermitian symmetric phase transition, and skin effect transition. Moreover, the topological states could exist on the double side localization characteristics in some regions.

To better judge the local effects of the system, we plot the phase diagrams and probability density spectra of the bulk as well as topological states, respectively. Figure 3(a) illustrates the phase diagram of the skin-effect phase transition in the bulk states, where yellow (purple) represents the right [R] (left [L]) localization of bulk states, corresponding to $\chi > 0 (< 0)$, indicating the right (left) localization of the skin effect. We can find that the system has two regions: The first region contains all the bulk states localized on the right side ($\chi > 0$) when $0 < \delta < \delta_{c1} = 0.332$, and there is no skin effect transition. In the second region, the skin effect displays the left-side localization (purple region of $\chi < 0$) in the region of $\delta > \delta_{c1}$,

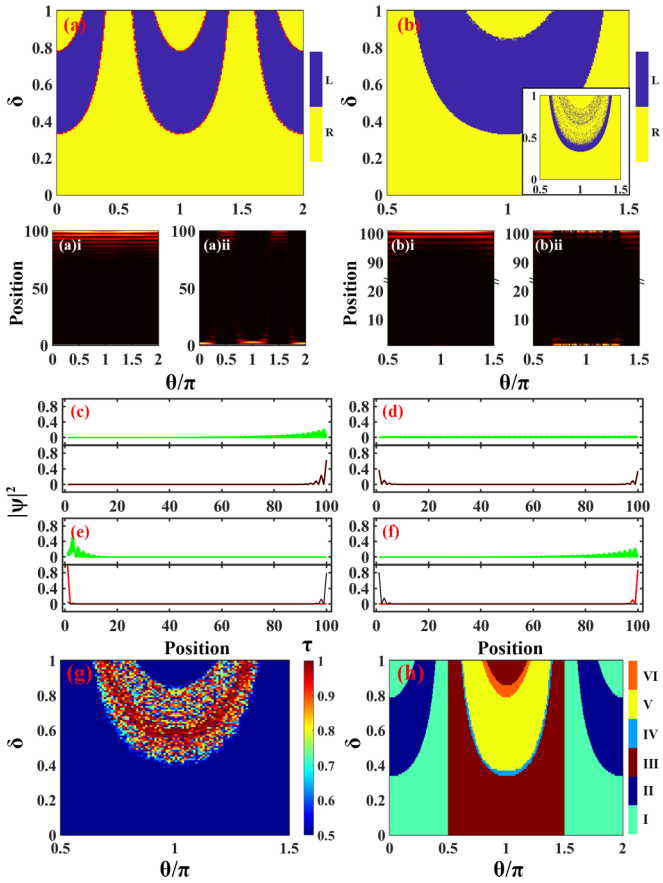

FIG. 3. (a), (b) The localization direction diagram spectra of bulk states and zero energy states. The yellow (purple) represents the right [R] (left [L]) localization. (a)(i), (ii) is the probability density spectra of $n = 32$ at $\delta = 0.2$ and $\delta = 0.6$. (b)(i), (ii) is the probability density spectra of $\delta = 0.3$ and $\delta = 0.6$. The color indicates the value of $|\psi|^2$, where black is $|\psi|^2 \approx 0$, and brighter colors indicate higher values of $|\psi|^2$. (c)–(f) The probability density spectra of $\theta = 0.6\pi$, $\theta = 0.65\pi$, and $\theta = 0.9\pi$ where $\delta = 0.7$, and $\theta = 0.9\pi$ at $\theta = 0.86$, respectively. (g) The R_{BBC} spectra of topological states. The color bar denotes the value of $\mathrm{R_{BBC}}(\tau)$. (h) The diagram spectra of six different phases.

and the system has the skin-effect phase transition. With the increase of δ, the region of left localization is decreased (purple region). In Figs. 3(a)(i) and 3(a)(ii), we provide the specific probability density spectra of $\delta = 0.2$ and $\delta = 0.6$ at $n = 32$, respectively. The color indicates the value of $|\psi|^2$, where black is $|\psi|^2 \approx 0$, and brighter colors show higher values of $|\psi|^2$. The position $j = 100$ represents the rightmost side and $j = 1$ corresponds to the leftmost side. For the case of Fig. 3(a)(i), all values of $|\psi|^2 > 0$ appear in the region close to $j = 100$, regardless of whether θ changes or not. It means that all eigenstates under the overall parameters show a tendency to be localized on the right side, and that there is no change in the local direction during the change of θ. However, when δ increases to 0.6, the regions with $|\psi|^2 > 0$ are alternately close to $j = 1$(L) or $j = 100$(R), forming a local trend of $L - R - L - R - L$. The system undergoes the skin-effect phase transition. These results are consistent with those in the phase diagram. From Eq. (12), we can get the expression of the condition of skin-effect phase transition with critical points being $\delta^2 = \frac{t_0^2 - t^2}{\cos^2\theta}$ and $\delta^2 = \frac{t_0^2 + t^2}{\cos^2\theta}$, i.e., $\delta_{c1} = \sqrt{t_0^2 - t^2}$ and $\delta_{c2} = \sqrt{t_0^2 + t^2}$. The results of phase transition condition and critical points are the same as the red lines in Fig. 3(a).

For the topological states, based on the energy spectra of Fig. 2, it can be seen that the two topological states may have the opposite localized directions. Thus, in Fig. 3(b), we plot the diagram spectra of localization direction of one topological state and the inset in the right corner shows the localized phase diagram of the another topological state. Figures 3(b)(i) and 3(b)(ii) describe the specific probability density spectra of $\delta = 0.3$ and 0.6, respectively. Because of Eq. (10), the topological sates appear in the region of $\theta \in [0.5\pi, 1.5\pi]$. For the region of $0 < \delta < 0.332$, all topological states are localized on the right side (yellow region), such as Fig. 3(b)(i). In the region of $0.332 < \delta < \delta_{c3} = 0.85$, the left-side localization appears [purple region]. When $\delta > 0.85$, the right-side localization region arises near $\theta = \pi$ and the left-side region is decreased. Different from the bulk states, when $\delta > 0.4$, the two topological states can be localized at the opposite directions, which can be called the double side localization effects [see Fig. 3(b)(ii)]. Comparing with the bulk states in Fig. 3(a), we can find that the topological states can be spatially separated from the bulk states in this region.

In Figs. 3(c)–3(f), we give four specific cases to observe the relationship of bulk states [green line] and two topological states [red and black lines]. Figure 3(c) shows the case of $\theta = 0.6\pi$ with $(t, \delta = 0.7)$. We can find that the bulk states display the right-side skin effect, whereas the two topological states are both localized on the right side and the wavefunctions coincide. When θ is equal to the phase condition, such as $\theta = 0.65\pi$ in Fig. 3(d), the bulk states are expended and the two topological states are both localized on the two sides simultaneously. For the case of $\theta = 0.9\pi$ when $\delta = 0.7$ [see Fig. 3(e)], the system exhibits the left-side skin effect, but one topological state is localized on the left side and the other is right. In this case, the right localized topological state can be separated from the bulk states. If $\delta = 0.86$, in the case of $\theta = 0.9\pi$, the left-side topological states can be separated, as shown in Fig. 3(f).

Moreover, we introduce the bulk-boundary correspondence ratio ($\mathrm{R_{BBC}}$) [45] to characterize the local direction change of the topological states. The definition is

$$\tau_l = 1 - \frac{|\langle \psi_{l,50} | \psi_{l,51} \rangle|}{2}, \tag{14}$$

where $|\psi_{l,50(51)}\rangle$ are two topological states that satisfy the self-normalization condition. If $\tau_l \approx 0.5$, the two topological states have the same localization and their wavefunctions coincide with each other. If $\tau_l \approx 1.0$, such states are localized at the opposite boundaries of the system, and their wavefunctions do not coincide. From Fig. 3(g), we can clearly find that in the blue region where $\tau = 0.5$, the topological states have the same localization. In the region of $0.4 < \delta < -\frac{t^2 + t_0}{\cos\theta}$, there will be $\tau \sim 1$. This indeed verifies that the local directions of the topological states are opposite in this region. This region is consistent with the result in Fig. 3(b). Finally, according to the above discussion, the system could have six different regions

TABLE I. The properties of different phases in Fig. 3(g) which are based on the localization directions of bulk states (bulk skin effect) and topological states.

Phase [Fig.3(g)]	Localization Direction		Phase [Fig.3(g)]	Localization Direction	
	Bulk states	Topological States (two)		Bulk states	Topological States (two)
I	Right		V	Left	Left
II	Left				Right
III	Right	Both Right	VI	Right	Left
IV	Left	Both Left			Right

I–VI, as shown in Fig. 3(g), and the specific properties are listed in Table I. We can find that the topological states can be separated in the region of V and VI.

IV. SUMMARY

In this work, we design one type of 1D semi–SSH lattice in which the intersite coupling in one direction is uniform, but in the other direction the intersite couplings change alternately. With the help of non-Hermitian quantum theory, we have performed an investigation about the skin effect and topological properties in this structure. Following the detailed theoretical demonstration, we have found that the skin effect can be tunable by adjusting the relative magnitudes of the intersite couplings in the two directions. However, the change of the skin effect is not necessarily accompanied by the variation of the topological zero-energy edge states. Therefore, in this work, we propose one new scheme to change the directionality of the topological edge states and the localized bulk states in the SSH lattice with nonreciprocal couplings, by controlling the appropriate intersite couplings. Meanwhile, this work promotes the understanding of the skin effects and topological properties in the 1D SSH lattices with nonreciprocal couplings.

ACKNOWLEDGMENTS

This work was financially supported by the LiaoNing Revitalization Talents Program (Grant No. XLYC1907033), the Natural Science Foundation of Liaoning province (Grant No. 2023-MS-072), the National Natural Science Foundation of China (Grants No. 11905027 and No. 12104183), and the Fundamental Research Funds for the Central Universities (Grants No. N2209005 and No. N2205015).

[1] C. Wu, N. Liu, G. Chen, and S. Jia, Non-Hermiticity-induced topological transitions in long-range Su-Schrieffer-Heeger models, Phys. Rev. A **106**, 012211 (2022).
[2] C. M. Bender, D. C. Brody, and H. F. Jones, Complex extension of quantum mechanics, Phys. Rev. Lett. **89**, 270401 (2002).
[3] C. M. Bender and S. Boettcher, Real spectra in non-Hermitian Hamiltonians having $\mathscr{P}\mathscr{T}$ symmetry, Phys. Rev. Lett. **80**, 5243 (1998).
[4] V. V. Konotop, J. Yang, and D. A. Zezyulin, Nonlinear waves in $\mathscr{P}\mathscr{T}$-symmetric systems, Rev. Mod. Phys. **88**, 035002 (2016).
[5] K. Kawabata, Y. Ashida, H. Katsura, and M. Ueda, Parity-time-symmetric topological superconductor, Phys. Rev. B **98**, 085116 (2018).
[6] S. Garmon and K. Noba, Reservoir-assisted symmetry breaking and coalesced zero-energy modes in an open $\mathscr{P}\mathscr{T}$-symmetric Su-Schrieffer-Heeger model, Phys. Rev. A **104**, 062215 (2021).
[7] J.-R. Li, L.-L. Zhang, W.-B. Cui, and W.-J. Gong, Topological properties in non-Hermitian tetratomic Su-Schrieffer-Heeger lattices, Phys. Rev. Res. **4**, 023009 (2022).
[8] L. Jin, Topological phases and edge states in a non-Hermitian trimerized optical lattice, Phys. Rev. A **96**, 032103 (2017).
[9] A. Yoshida, Y. Otaki, R. Otaki, and T. Fukui, Edge states, corner states, and flat bands in a two-dimensional $\mathscr{P}\mathscr{T}$-symmetric system, Phys. Rev. B **100**, 125125 (2019).
[10] X. Zhu, H. Wang, S. K. Gupta, H. Zhang, B. Xie, M. Lu, and Y. Chen, Photonic non-Hermitian skin effect and non-Bloch bulk-boundary correspondence, Phys. Rev. Res. **2**, 013280 (2020).
[11] K. Xu, X. Zhang, K. Luo, R. Yu, D. Li, and H. Zhang, Coexistence of topological edge states and skin effects in the non-Hermitian Su-Schrieffer-Heeger model with long-range nonreciprocal hopping in topoelectric realizations, Phys. Rev. B **103**, 125411 (2021).
[12] S. M. Rafi-Ul-Islam, Z. B. Siu, H. Sahin, C. H. Lee, and M. B. A. Jalil, Critical hybridization of skin modes in coupled non-Hermitian chains, Phys. Rev. Res. **4**, 013243 (2022).
[13] L. Feng, R. El-Ganainy, and L. Ge, Non-Hermitian photonics based on parity-time symmetry, Nat. Photon. **11**, 752 (2017).
[14] Y. Wu, B. Zhu, S.-F. Hu, Z. Zhou, and H.-H. Zhong, Floquet control of the gain and loss in a PT-symmetric optical coupler, Front. Phys. **12**, 121102 (2017).
[15] S. Weidemann, M. Kremer, T. Helbig, T. Hofmann, A. Stegmaier, M. Greiter, R. Thomale, and A. Szameit, Topological funneling of light, Science **368**, 311 (2020).
[16] A. Regensburger, C. Bersch, M. A. Miri, G. Onishchukov, D. N. Christodoulides, and U. Peschel, Parity-time synthetic photonic lattices, Nature (London) **488**, 167 (2012).
[17] M. Parto, S. Wittek, H. Hodaei, G. Harari, M. A. Bandres, J. Ren, M. C. Rechtsman, M. Segev, D. N. Christodoulides, and M. Khajavikhan, Edge-mode lasing in 1D topological active arrays, Phys. Rev. Lett. **120**, 113901 (2018).
[18] F. Koch and J. C. Budich, Quantum non-Hermitian topological sensors, Phys. Rev. Res. **4**, 013113 (2022).
[19] J. C. Budich and E. J. Bergholtz, Non-Hermitian topological sensors, Phys. Rev. Lett. **125**, 180403 (2020).
[20] A. McDonald and A. A. Clerk, Exponentially-enhanced quantum sensing with non-Hermitian lattice dynamics, Nat. Commun. **11**, 5382 (2020).
[21] S. Yao and Z. Wang, Edge states and topological invariants of non-Hermitian systems, Phys. Rev. Lett. **121**, 086803 (2018).
[22] S. Yao, F. Song, and Z. Wang, Non-Hermitian Chern bands, Phys. Rev. Lett. **121**, 136802 (2018).
[23] V. M. Martinez Alvarez, J. E. Barrios Vargas, and L. E. F. Foa Torres, Non-Hermitian robust edge states in one dimension:

Anomalous localization and eigenspace condensation at exceptional points, Phys. Rev. B **97**, 121401(R) (2018).

[24] C. H. Lee and R. Thomale, Anatomy of skin modes and topology in non-Hermitian systems, Phys. Rev. B **99**, 201103(R) (2019).

[25] Y. Xiong, Why does bulk boundary correspondence fail in some non-Hermitian topological models, J. Phys. Commun. **2**, 035043 (2018).

[26] T. S. Deng and W. Yi, Non-Bloch topological invariants in a non-Hermitian domain wall system, Phys. Rev. B **100**, 035102 (2019).

[27] F. Song, S. Yao, and Z. Wang, Non-Hermitian topological invariants in real space, Phys. Rev. Lett. **123**, 246801 (2019).

[28] K. Yokomizo and S. Murakami, Non-Bloch band theory of non-Hermitian systems, Phys. Rev. Lett. **123**, 066404 (2019).

[29] L. Xiao, T. S. Deng, K. K. Wang, G. Y. Zhu, Z. Wang, W. Yi, and P. Xue, Observation of non-Hermitian bulk-boundary correspondence in quantum dynamics, Nat. Phys. **16**, 761 (2020).

[30] P.-C. Cao, Y.-G. Peng, Y. Li, and X.-F. Zhu, Phase-locking diffusive skin effect, Chin. Phys. Lett. **39**, 057801 (2022).

[31] A. Ghatak, M. Brandenbourger, J. van Wezel, and C. Coulais, Observation of non-Hermitian topology and its bulk-edge correspondence in an active mechanical metamaterial, Proc. Natl. Acad. Sci. USA **117**, 29561 (2020).

[32] E. J. Bergholtz, J. C. Budich, and F. K. Kunst, Exceptional topology of non-Hermitian systems, Rev. Mod. Phys. **93**, 015005 (2021).

[33] T. Helbig, T. Hofmann, S. Imhof, M. Abdelghany, T. Kiessling, L. W. Molenkamp, C. H. Lee, A. Szameit, M. Greiter, and R. Thomale, Chiral voltage propagation and calibration in a topolectrical Chern circuit, Nat. Phys. **16**, 747 (2020).

[34] L. Xie, L. Jin, and Z. Song, Antihelical edge states in two-dimensional photonic topological metals, Sci. Bull. **68**, 255 (2023).

[35] F. K. Kunst, E. Edvardsson, J. C. Budich, and E. J. Bergholtz, Biorthogonal bulk-boundary correspondence in non-Hermitian systems, Phys. Rev. Lett. **121**, 026808 (2018).

[36] C. Yin, H. Jiang, L. Li, R. Lü, and S. Chen, Geometrical meaning of winding number and its characterization of topological phases in one-dimensional chiral non-Hermitian systems, Phys. Rev. A **97**, 052115 (2018).

[37] C. Yuce and H. Ramezani, Topological states in a non-Hermitian two-dimensional Su-Schrieffer-Heeger model, Phys. Rev. A **100**, 032102 (2019).

[38] K. Kawabata, K. Shiozaki, M. Ueda, and M. Sato, Symmetry and topology in non-Hermitian physics, Phys. Rev. X **9**, 041015 (2019).

[39] G. Marinello and M. P. Pato, Random non-Hermitian tight-binding models, J. Phys.: Conf. Ser. **738**, 012040 (2016).

[40] O. Bohigas and M. P. Pato, Non-Hermitian β-ensemble with real eigenvalues, AIP Adv. **3**, 032130 (2013).

[41] S. M. Rafi-UI-Islam, H. Sahin, Z. B. Siu, and M. B. A. Jalil, Interfacial skin modes at a non-Hermitian heterojunction, Phys. Rev. Res. **4**, 043021 (2022).

[42] Z.-Q. Zhang, H. Liu, H. Liu, H. Jiang, and X. C. Xie, Bulk-boundary correspondence in disordered non-Hermitian system, Sci. Bull. **68**, 157 (2023).

[43] W. J. Geng, Y.-J. Wang, Z.-X. Zhang, J. Cao, W.-X. Cui, and H.-F. Wang, Separable zero energy topological edge states and nonzero energy gap states in the nonreciprocal Su-Schrieffer-Heeger model, Phys. Rev. B **108**, 144109 (2023).

[44] Q.-B. Zeng and R. Lü, Real spectra and phase transition of skin effect in nonreciprocal systems, Phys. Rev. B **105**, 245407 (2022).

[45] X.-R. Wang, C.-X. Guo, and S.-P. Kou, Defective edge states and number-anomalous bulk-boundary correspondence in non-Hermitian topological systems, Phys. Rev. B **101**, 121116(R) (2020).